RASĀYAN *J. Chem.*
Vol. 19 | No. 4 | 2037-2048 | October-December | 2026
ISSN: 0974-1496 | e-ISSN: 0976-0083 | CODEN: RJCABP
http://www.rasayanjournal.com
http://www.rasayanjournal.co.in

SYNTHESIS, CHARACTERIZATION, AND MULTIFUNCTIONAL APPLICATIONS OF 2-NITRO HYDRAZIDE AND 4-NITRO HYDRAZIDE STABILIZED SILVER NANOPARTICLES FOR CATALYTIC DYE DEGRADATION, METAL ION DETECTION, ANTICANCER, AND ANTIMICROBIAL ACTIVITIES

Y. Desai[1], T. Barot[1,✉], S. Patel[1], N. Pomal[2], D. Patni[3], P. Patel[1], and H. Kardani[1]

[1]Department of Chemistry, Mehsana Urban Institute of Sciences, Ganpat University, Ganpat Vidhyanagar-384012, (Gujarat) India

[2]Department of Physical and Chemical Sciences, Faculty of Science, Sigma University, Waghodia, Vadodara-390019, (Gujarat) India

[3]Department of Life Sciences, Faculty of Science, Sigma University, Waghodia, Vadodara-390019, (Gujarat) India
✉Corresponding author: tdp02@ganpatuniversity.ac.in

ABSTRACT

Silver nanoparticles were produced by a chemical reduction process, wherein Ag^+ ions from $AgNO_3$ were converted to metallic Ag^0 utilising an appropriate reducing agent such as hydrazine. By acting as a stabilising and capping agent, the synthesised hydrazine-based ligand maintained the stability of the nanoparticles and prevented agglomeration. The synthesis of 2-nitrohydrazide-capped silver nanoparticles (2-NHAgNPs) was carried out using the conventional method, while the synthesis of 4-nitrohydrazide-capped silver nanoparticles (4-NHAgNPs) was performed using the ultrasonic method. Silver nanoparticles were synthesised via a typical one-pot chemical reduction method. Comprehensive characterisation using UV-Visible Spectroscopy, Fourier Transform Infrared Spectroscopy, Transmission Electron Microscopy, Particle size distribution, and zeta potential confirmed the successful formation of 2-NHAgNPs and 4-NHAgNPs. Furthermore, the 2-NHAgNPs and 4-NHAgNPs exhibit remarkable anticancer effects against the human Brest cancer cell line MCF-7, different dye degradation, various sensing of metal ions and gram-positive and gram- negative antimicrobial activity.

Keywords: Silver Nanoparticles, Anti-cancer, 2-NHAgNPs, 4-NHAgNPs.

RASĀYAN *J. Chem.*, Vol. 19, No.4, 2026

INTRODUCTION

Silver in its various forms has long been recognised for its strong antimicrobial properties. Throughout history, it has been used both alone and in combination with other technologies to effectively inhibit the growth of harmful microorganisms. Silver nanoparticles (AgNPs) are classified as nanomaterials with dimensions that generally range from 1 to 100 nanometers. They possess a significantly larger surface area and reactivity compared to bulk silver. AgNPs have been extensively explored for applications in targeted drug delivery, diagnostic systems, biosensing, and imaging technologies.[1] The scheme, production of materials at the nanoscale level to provide features that can be appropriately used for applications that are required, is referred to as nanotechnology.[2] Due to their smaller size, high monodispersity, and physicochemical characteristics, metallic nanoparticles (MNPs) have generated a lot of research.[3] NPs are created using a variety of methods, such as chemical, biological, and physical. For the synthesis of AgNPs, conventional methods like chemical and physical procedures are suggested.[4] Silver nanoparticles have anti-inflammatory, antiviral and anti-diabetic properties in biomedicine.[5] Metallic nanoparticles can be synthesized utilization two main strategies: top-down and bottom-up. These

http://doi.org/10.31788/RJC.2026.1949946

methods differ in how the nanostructures are formed, either by assembling atoms and molecules into nanoscale materials (bottom-up) or by breaking down bulk materials into smaller particles **(**top-down). Top-down approaches produce nanoparticles by breaking down bulk metallic silver, either in solid or aerosolised form, into nanoscale particles. This process enables the formation of stable silver nanoparticles (AgNPs) through controlled size reduction.[6] These include physical techniques such as ball milling, laser ablation, and sputtering. Bottom-up approaches involve building nanoparticles by assembling silver atoms into stable nanostructures using various synthesis techniques. The third approach, biological synthesis, involves producing nanoparticles using biological materials or living organisms. This includes fungal or bacterial-mediated synthesis, as well as methods that utilise natural extracts as reducing and stabilising agents. Biologically synthesised AgNPs have shown excellent solubility, high yield, and strong stability.[1] Cyclic rings of atoms with at least one heteroatom are known as heterocyclic compounds. Although nitrogen, oxygen, and sulfur are the most prevalent heteroatoms, heterocyclic rings containing other heteroatoms such as phosphorus, iron, magnesium, selenium, etc. are also frequently found.[7] Heterocyclic compounds include a wide variety of vitamins, medications, biomolecules, natural products, and biologically active substances such as antibiotics, antitumor, anti-inflammatory, antimalarial, antidepressants, antibacterial, antiviral, anti-diabetic, antifungal, herbicidal, fungicidal and insecticidal agents.[8] Chemistry is typically one of the more complicated areas of chemistry.[9] Degradation of the dye molecule into innocuous components is difficult due to its chemical composition, which provides it with exceptional longevity. Because of their many physical and chemical properties, metallic nanoparticles can be used by researchers in a wide range of industries, as well as food**,** textiles, healthcare**,** the environment, agriculture, and more.[10] The production of silver nanoparticles was examined using TEM, Zeta potential, UV-Visible spectroscopy, and other techniques to determine their morphological characteristics, including size, shape, and surface charge. Dye degradation was further investigated using the produced AgNPs. The improved degradation potential of chemically generated silver nanoparticles when mixed with sodium borohydride for Blue and Rhodamine dyes, both independently and in combination (simultaneously).[11] Physical, chemical, and biological mechanisms can create the nanoparticles needed for the catalytic breakdown of textile colours. Silver nanoparticles require a lot of energy, whereas biological methods use plants, bacteria**,** fungi and algae as materials.[12] Chemical synthesis of silver nanoparticles is more flexible and uses a method that yields stable nanoparticles in terms of size and shape.[13] Numerous studies have employed the catalytic activity of nanoparticles against a spectrum of harmful dyes, like Auramine O, Thymol Blue, Rhodamine B dye, Congo Red dye, Phloxine B, Methyl Orange, more. Silver nanoparticles have been shown to degrade a variety of colours by up to 90-100%. Researchers recently highlighted the green-produced AgNPs' effective dye degradation capability for Methyl orange, Methyl Red and Congo Red (separately).[14] The different study, synthetic silver nanoparticles derived from Sophora mollis leaf extract demonstrated 88% Methylene Blue degradation in 160 minutes.[15] AgNPs have the promising ability to degrade methylene blue, according to a different study.[16] According to observations, the literature exclusively focuses on the catalytic activity of silver nanoparticles on specific colours. Mercury is a dangerous element in the environment and a heavy metal that may be detrimental to human health**.** According to the WHO, mercury is one of the top 10 compounds or chemical groupings that pose the biggest threat to public health.[17] It contains up to 80% mercury, which is released into the environment in different forms. Human Cu^{+2} ion concentration can be dangerous and lead to major conditions such as hypoglycemia and dyslexia.[18] Cu^{2+} ions are produced by multiple companies during their manufacturing processes, which can enter the food chain and accumulate in humans. The most common hazardous heavy metal in the environment that has been detected in our atmosphere is lead (Pb). Mercury, Arsenic, Chromium, and Cadmium, it is also regarded as one of the five heavy metals that are frequently detected in water.[19] Lead is still used in the production of paint, automobile batteries, and lead metal electrode recovery. Many techniques, such as cold vapor atomic absorption,[20] cold vapor atomic fluorescence spectroscopy,[21] atomic absorption spectroscopy,[22] inductively coupled plasma atomic emission spectroscopy,[23] electro thermal atomic absorption spectroscopy, atomic fluorescence spectrometry, fluorescent probes,[24] inductively couple plasma- mass spectrometry,[25] and electrochemical detection,[26] have been used to determine the mercury, copper, lead, and cobalt contents of different samples. One of the most important aspects of modern technology is the

creation of sensors to measure, track, and identify heavy metals in environmental samples. Therefore, colourimetric sensing of cobalt, copper, lead, and mercury using AgNPs is a highly active, effective, quick, and environmentally friendly method. The potential of the produced silver nanoparticles as colourimetric sensors for identifying Co, Cu, Pb, and Hg ions is also examined in this study. This study differs from earlier research in several ways.[17] There are numerous papers on the sensing and detection of hazardous metal ions utilising different synthetic (chemical, physical**,** and biogenic) techniques.[27] The simplest method for producing AgNPs is to chemically reduce silver salts using sodium citrate (SC). SC serves as both a coordinating and a reducing agent. Silver nanoparticles have a realm of colourimetric sensors due to their special characteristics. Ag nanoparticles exhibit distinct optical properties and a high excitation coefficient in the visible spectrum.[27] The current study reports on the use of sodium citrate-stabilised silver nanoparticles (AgNPs) for UV-Vis spectroscopic sensing and detection of several metal ions **(**Co^{2+}, Pb^{2+}, Zn^{2+}, Ba^{2+}, Ca^{2+}, Mg^{2+}, K^{+}, Sr^{2+}, and Zr^{2+}**)** in aqueous solution.

EXPERIMENTAL

Material and Methods

Aniline, sodium nitrate, sodium azide, hydrazine hydrate, all metal salts, and silver nitrate were purchased from Sigma-Aldrich. Other solvents, chemical and reagent grade obtained from a chemical supplier and used without purification. TLC plates with fluorescence activity (F-254) were provided by Merck. The micropipette (VAR VOL 100-1000 µl, Kasablanka, Mumbai) and magnetic stirrer (REMI-MLH) were utilised. Before being used, every piece of glassware was carefully calibrated. A VEGO model VMP-DS (Mumbai) was used to calculate uncorrected melting points. Electrospray ionisation (ESI) mass spectra were obtained on a SHIMADZU Nexera 2020 using a Micro Mass Quarter-2 instrument. A two-channel 400 MHz NMR spectrometer was used to record the NMR spectra, and ChemDraw Professional software was used to create the chemical structure and nomenclature. Research and testing were conducted using the Transmission Electron Microscope (model name JEOL, JEM-2100). UV-Vis spectra were recorded using a SCHIMADZU-1900 system. The cell line utilised in the anti-cancer activities was MCF-7.

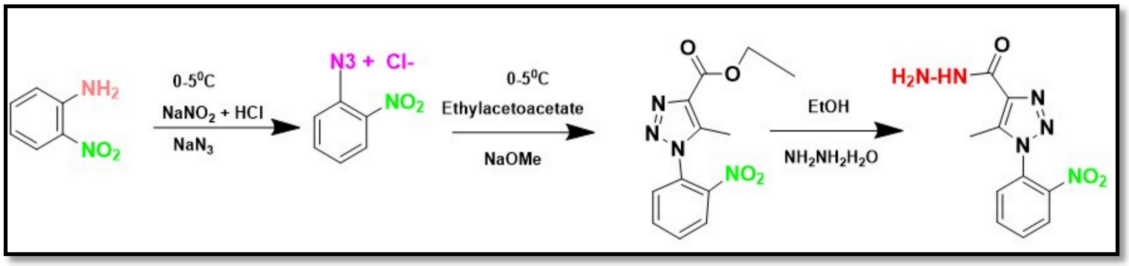

Scheme-1: (Synthesis of 2-NHAgNPs)

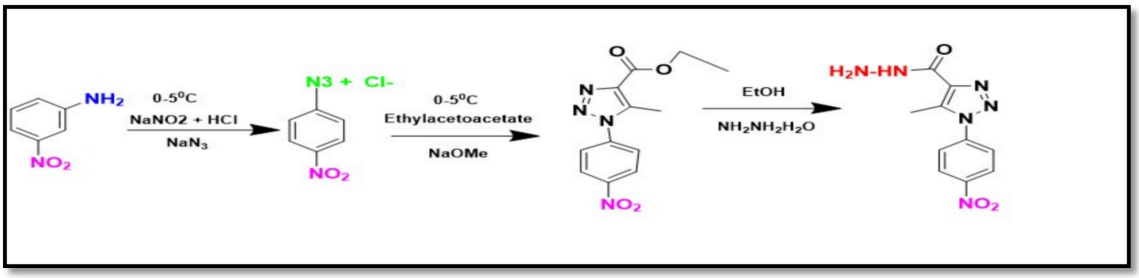

Scheme-2: (Synthesis of 4-NHAgNPs)

Synthesis: Preparation of 5-methyl-1-phenyl-1H-1,2,3-triazole-4-carbohydrate and its Derivatives (Scheme -1 and Scheme-2)

Preparation of Various Azide Derivatives of Aniline

According to a published process (Bhola 2019), hydrochloric acid (6 mL) and distilled water (20 mL) were added to a round-bottom flask with three necks, a mechanical stirrer, and a cooling system to create the azide derivatives. After cooling the mixture to 0 °c, the corresponding aniline derivative (5.0 g, 0.053

mol) was added dropwise while the temperature was kept between 0-5 °c. After adding an already prepared sodium nitrate solution (3.65 g, 0.053 mol) gradually, sodium azide (3.44 g, 0.053 mol) was added dropwise while being continuously stirred at 0-5 °c.

Preparation of Ethyl 5-methyl-1-phenyl-1H-1,2,3-triazole-4-carboxylate

Ethyl acetoacetate (9.1 g, 0.007 mol) was added to methanol in an inert atmosphere to treat ethyl 5-methyl-1-phenyl-1H-1,2,3-triazole-4-carboxylate azide (4.2 g, 0.035 mol). After cooling the reaction mixture to 0 °C, sodium methoxide (3.7 g, 0.07 mol) was gradually added. During complete addition, the mixture was stirred and allowed to reach room temperature while thin-layer chromatography (TLC) was used to observe the reaction's progress. When the reaction was finished, a solid precipitate was formed by pouring the reaction mixture into ice-cold water. To obtain the required compounds 7a-d (6.2 g, 76.68%), the crude product was filtered, extensively cleaned with water, and recrystallised from ethanol.

Preparation of 5-methyl-1-phenyl-1H-1,2,3-triazole-4-carbohtdrazide (8a-d)

Ethyl 5-methyl-1-phenyl-1-H-1,2,3-triazole-4-carboxylate (6 g, 0**.**0259 mol**)** was dissolved in ethanol (30 mL) to create the carbohydrazide derivatives. After adding Hydrazine hydrate to the solution dropwise, the reaction mixture was refluxed for six hours at80 ^{0}C. The mixture was allowed to cool to room temperature once the reaction was finished, and the resultant solid was filtered out. The carbohydrazide derivatives 8a-d (5 g, 88.80 %) were obtained by thoroughly cleaning and drying the crude product with water.

2-Nitrohydrazide

Solid, pale yellow to orange (88.80% yield). M.P.: 97 ^{0}C Chemical Formula: $C_{13}H_{19}N_6O3$ ^{1}H- NMR: (δ in ppm) 9.82 (S, NH), 4.49 (S-NH_2), 2.50 (S-CH_3), 7.94-7.96 (M-4-Ar-H). ^{13}C-NMR: δ = 138, 145.7, 126.4, 130, 135.4, 128.11, 9.18, 128.11, 135.4, 160.38.ESI-MS (m/z): 262.16

3-Nitrohydrazde

Solid Pale yellow to orange (88.80% yield). M.P.: 106 ^{0}C Chemical Formula: $C_{13}H_{19}N_6O3$ ^{1}H- NMR: (δ in ppm) 9.63 (S, NH), 4.4 (S- NH_2), 2.50 (S-CH_3), 8.28-8.30 (M-4-Ar-H) ^{13}C-NMR: δ 136.6, 123.8, 126.7, 114, 126.7, 150, 9.7, 137.8, 136.6, 161. ESI-MS (m/z): 262.16

Synthesis of 2-nitrohydrazide-capped Silver Nanoparticles (2-NHAgNPs) (Conventional Method)

Silver nanoparticles were synthesised via a typical one-pot chemical reduction method. Briefly, 25 mL of 1 millimeter aqueous solution of 2-nitrohydrazide (2-NH) was transferred to a conical flask containing 25 mL of 1 millimeter silver nitrate ($AgNO_3$) solution (corresponding to 2.7 mg of Ag^+ ions). The reaction mixture was subjected to vigorous magnetic stirring at room temperature. The stirring was continuous; a distinct and permanent turbid yellow colouration signified the formation of silver nanoparticles**.** After completion of the reaction, the colloidal solution was maintained at 4 ^{0}C for further investigation and stability studies (Fig.-1).

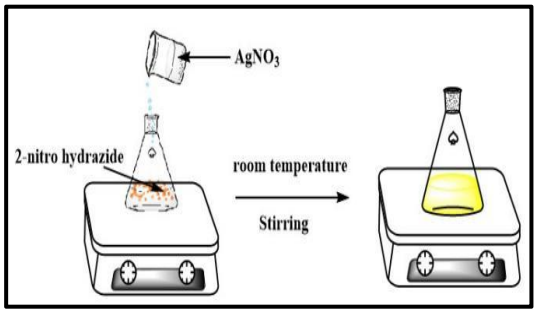

Fig.-1: Synthesis of 2-NHAgNPs

Synthesis of 4-nitrohydrazide-capped Silver Nanoparticles (4-NHAgNPs) (Ultrasonic Method)

A 50 mL conical flask with 20 mL of dimethylformamide (DMF) was filled with 10 mL of 1 millimeter 4-nitro hydrazide (4-NH) solution. To ensure complete dissolution and homogeneity of the ligand solution, the mixture was rapidly stirred for a duration of five minutes. The reaction mixture was then continuously stirred at room temperature while 10 mL of 1-millimetre $AgNO_3$ solution was added

dropwise. The reaction system was exposed to ultrasonic irradiation using an ultrasonic reactor for 25 minutes right after the addition of the silver precursor. Acoustic cavitation effects caused the solution's temperature to progressively rise and stabilise between 40 and 50 °C during sonication. Ag^{+} ions were reduced to metallic silver (Ag^{0}) with the help of the ultrasonic energy. As a result of surface Plasmon resonance, the initially translucent and colourless solution progressively turned bright yellow, signifying the formation of AgNPs. After the sonication process was complete, the reaction mixture solution was allowed to naturally cool to ambient temperature before additional characterisation (Fig.-2).

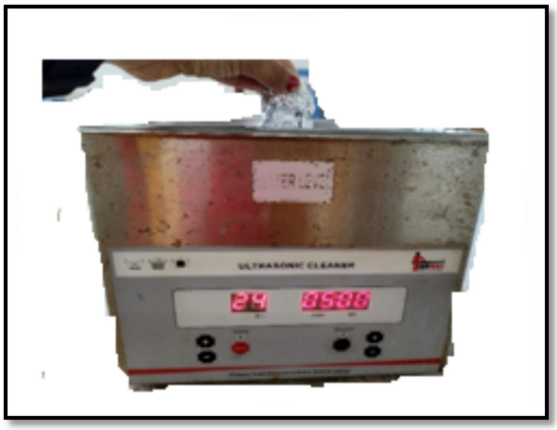

Fig.-2: Synthesis of 4-NHAgNPs

RESULTS AND DISCUSSION

Characterization

The UV-Visible approach has been commonly used for evaluating and verifying the metal nanoparticle composition. In the Ultraviolet-Visible Spectrum 2-NHAgNPs absorption peak about 414 nm was confirmed (Fig.-3A).

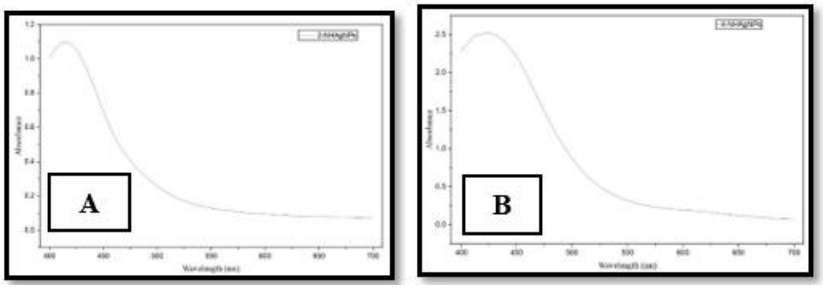

Fig.-3: UV –Visible Spectrum of (A) 2-NHAgNPs, (B) 4-NHAgNPs

The UV-Visible approach has been commonly used for evaluating and verifying the metal nanoparticles composition. In the Ultraviolet-Visible Spectrum 4-NHAgNPs absorption peak about 434 nm was confirmed (Fig.-3B). Transmission Electron Microscopy were used to analyse the morphology and particle size of the produced 2-nitrohydrazide silver nanoparticles (2-NHAgNPs). The TEM micrographs show that the nanoparticles have a modest polydispersity and are primarily spherical in shape. Because of their high surface energy, metal nanoparticles frequently exhibit well-dispersed particles with some degree of aggregation. Particle size is estimated to be between 10 and 50 nm based on TEM pictures with scale bars of 50 and 100 nm, with the majority of nanoparticles falling between the 20-40 nm size range. The darker contrast observed in the TEM images corresponds to the metallic silver core, confirming the formation of dense nanoparticles. The aggregation of smaller nanoparticles during synthesis or drying on the TEM grid may be the cause of some bigger particles shown in the micrograph (Fig.-4 (a, b)).

2-nitrohydrazide successfully works as a stabilising and capping agent during the synthesis of AgNPs, to prevent excessive particle growth according to the comparatively uniform morphology and nanoscale size distribution. Zeta potential distribution of the 2-NHAgNPs sample dispersed showing a single peak with a

mean Zeta potential of +8.5 mV, indicating moderately stable particles with a slightly positive surface charge Fig.-4 (c).

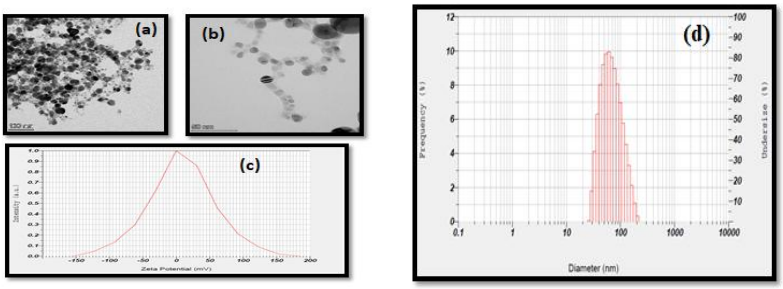

Fig.-4 (a, b): TEM Image of 2-NHAgNPs, (c) Zeta Potential, (d) Particle Size

The analysis of 2-NHAgNPs mean particle size is 73.7 nanometers with a mode diameter of 60.6 nm and a standard deviation of 34.1 nm. The Z-average particle size was calculated to be 45.8 nm, which is the hydrodynamic diameter of the particle in the solvent. The polydispersity index value of 0.464 indicates that the particles exhibit a moderately polydisperse distribution Fig.-4 (d).

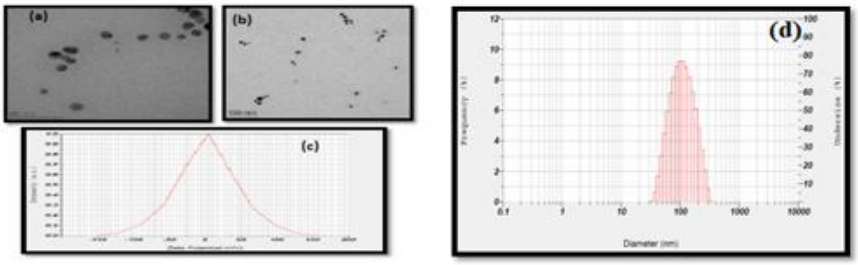

Fig.-5: (a, b) TEM Image of 4-NHAgNPs, (c) Zeta Potential, (d) Particle Size

Transmission Electron Microscopy picture of the created 4-NHAgNPs at various magnifications. The creation of mostly spherical nanoparticles with diameters in the nanometer range is visible in the pictures. The majority of particles are widely distributed, with a small amount of aggregation in specific areas. The nanoscale dispersion is consistent with the estimated particle size of 20-80 nm based on the TEM pictures. The scale bars, which represent 50 and 100 nm, show the dispersion and shape of the nanoparticles Fig.-5 (a, b). Zeta potential distribution profile of the 4-NHAgNPs sample dispersed in DMF, measured using a zeta potential analyser at 25 ^{0}c. The distribution shows a single peak with a mean Zeta potential value of +2.9 mV Fig.-5 (c). Particle size distribution histogram of the 4-NHAgNPs sample dispersed in DMF, measured using a particle size analyser at 24.9. The distribution shows a particle size of 118.5 nanometers, with a mode diameter of 99.1 nanometers and standard deviation of 55.6 nanometers, indicating nano-sized particles with polydispersity distribution Fig.-5 (d).

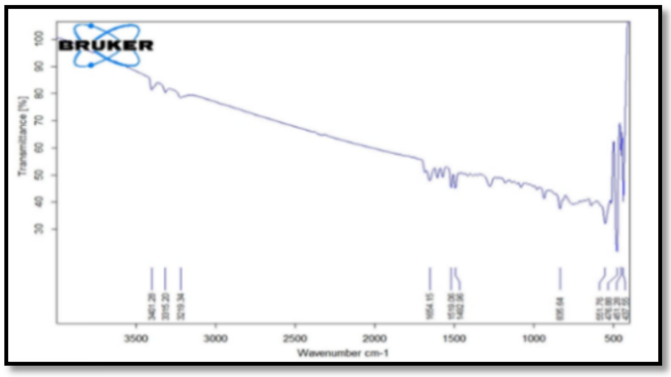

Fig.-6: FT-IR Spectra of 4- NH

The hydrazine groups' N-H stretching vibrations are represented by distinctive bands in the FTIR spectra of 4-nitrohydrazine at 3401, 3322, and 3219 cm^{-1}. The peak at 1654 $cm^{-1}$is attributions to N-H bending. Asymmetric –NO2 stretching and aromatic C=C vibrations are confirmed by the strong absorption at 1519 $cm^{-1}$and 1492 cm^{-1}. Para-substituted aromatic C-H bending is indicated by the band at 835 cm^{-1}. Furthermore, N-N stretching and vibration are attributed to peaks in the 551-437 cm^{-1} (Fig.-6).

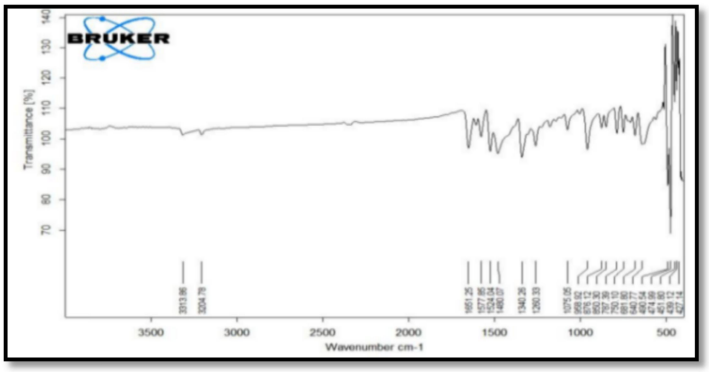

Fig.-7: FT-IR Spectra of 2- NH

N-H stretching vibrations are represented by a distinctive band in the FTIR spectra of 2-nitrohydrazine at 3313 and 3204 cm^{-1}; N-H bending is the peak at 1651 cm^{-1}. Asymmetric and symmetric stretching of the–NO2 group are confirmed by strong absorption at 1578 cm^{-1} and 1524 cm^{-1}, as well as a band at 1340 cm^{-1}. Aromatic C=C stretching the observed at 1480 cm^{-1}, whilst C-N and N-N stretching vibrations are present in the 958-681 cm^{-1} region. These show aromatic C-H bending. N-N vibrations are responsible for the lower-frequency band (610-427 cm^{-1}) (Fig.-7).

Catalytic Dye Degradation using Silver Nanoparticles

The catalytic activity of the synthesised 2-nitrohydrazide-stabilised silver nanoparticles (2-NHAgNPs) was evaluated via the reduction of different organic dyes as well as Methyl Orange**,** Methylene Blue**,** Congo Red, Rhodamine B, and Methyl Red in aqueous medium. The degradation experimentation was carried out at room temperature using freshly prepared sodium borohydride as a reducing agent. In a typical experiment, 2 mL of dye solution (0.1 mM) was mixed with .5 mL of freshly prepared $NaBH_4$ solution (100 mM) under continuous stirring. Subsequently, 5 mg of synthesised 2-nitrohydrazide silver nanoparticles was added to the reaction mixture to initiate the catalytic degradation process. The reaction was performed in a 1 cm path length quartz cuvette, and the progress of the reaction was monitored using an Ultraviolet-Visible Spectrophotometer in the wavelength range of 200 to 800 nanometers. At regular intervals, a reduction in each dye's distinctive absorption peaks was observed.

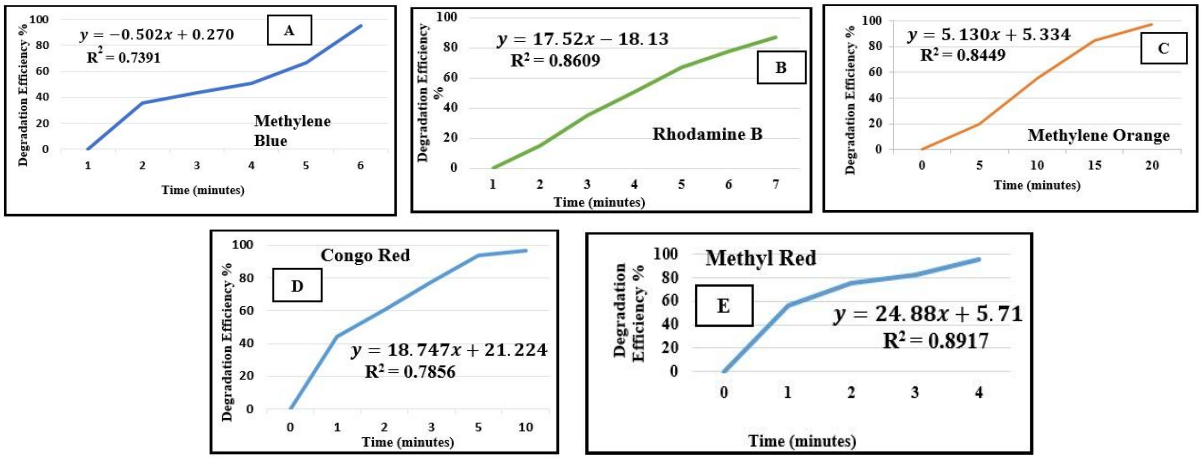

Fig.-8: Degradation Rate of (a) MB, (b) RB, (c) MO, (d) CR, and (e) MR
Dye Degradation → SDG-3

Sensing of Different Metal Ions

Using UV-Visible spectroscopy, the metal ion sensing behaviour of the produced silver nanoparticles was methodically examined in the presence of different metal nitrate solutions, such as Co^{2+}, Pb^{2+}, Zn^{2+}, Ba^{2+}, Ca^{2+}, Mg^{2+}, K^{+}, Sr^{2+}, and Zr^{2+} ions. AgNPs' distinctive surface plasmon resonance (SPR) band was detected at around 413-414 nm. Significant changes in absorbance intensity were noted upon the addition of various metal ions, suggesting unique patterns of interaction between the nanoparticles and metal ions. Co^{2+} showed a markedly increased absorbance (1.098) among all measured ions, indicating powerful interaction and high selectivity toward cobalt ions. Zn^{2+} and Ca^{2+} ions, on the other hand, displayed comparatively lower absorbance values (~ 0.089), indicating some interaction with the surface of the nanoparticle. Pb^{2+} (0.110), Zr^{2+} (0.111), Sr^{2+} (0.103), Mg^{2+} (0.097), Ba^{2+} (0.104), and K^{+} (0.148) all showed moderate reactions. Differences in ionic charge density, coordination ability, and contact strength with the AgNPs surface can be connected to the observed variation in SPR intensity. Overall, the findings show that AgNPs have sensitive and selective detection behaviour, with a stronger reaction to Co^{2+} ions than to other metal ions.

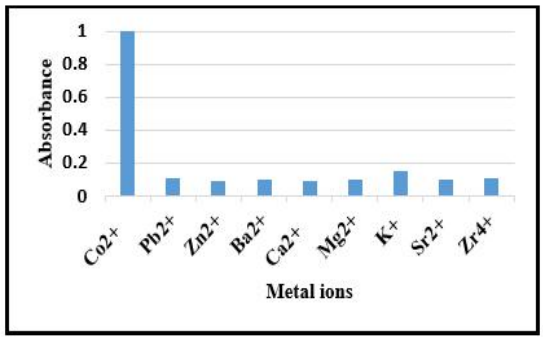

Fig.-9: Metal Ion Sensing Capability of the Stabilised Silver Nanoparticles With Respect to the Change in Absorption Ratio

Antimicrobial Activity

Silver and AgNPs have a bactericidal action. According to several studies, AgNPs may bind to the cell membrane surface, disrupting the cell's permeability and respiration processes. Compared to bigger AgNPs, smaller AgNPs would have a greater bactericidal impact due to their higher surface area accessible for interaction. AgNPs may potentially be able to enter the bacteria in addition to interacting with the membrane surface.[28] The antimicrobial activity of 2-nitrohydrazide silver nanoparticles (2-NH-AgNPs) and 4-nitrohydrazide silver nanoparticles (4-NH-AgNPs) was analysed using the agar well diffusion method against Staphylococcus aureus, Bacillus subtilis, E. coli, Pseudomonas aeruginosa, and Aspergillus Niger.

The antibacterial results definitely show that 4-nitrohydrazide AgNPs are much more active against both Gram-positive and Gram-negative bacterial with fungal strains than 2-nitrohydrazide AgNPs. A dose-dependent characteristic is indicated by the activity increasing with concentration. With the maximum inhibition zones of 23 mm and 24 mm, respectively, at 100% concentration, pseudomonas aeruginosa and Aspergillus Niger, demonstrated the greatest vulnerability to 2-nitro AgNPs among all studied bacteria. Strong antibacterial activity was also seen against E. coli (21 millimetres) and Staphylococcus aureus (22.6 millimetres), although Bacillus subtilis (12.3 millimetres) showed relatively little action. On the other hand, at lower doses (25-75 %), 2-nitro AgNPs showed weak to moderate antibacterial efficacy and no inhibition against S. aureus. The action was limited even at 100 % concentration (maximum 15 mm for E. coli), indicating lower efficacy in comparison to the 4-nitro derivative. The agar well diffusion method was used to assess the antibacterial activity of produced 2-nitrohydrazide silver nanoparticles (2-NH-AgNPs) and 4-nitrohydrazide silver nanoparticles (4- NH- AgNPs). On nutritional agar and potato dextrose agar, respectively, pure cultures of Staphylococcus aureus, Bacillus subtilis, Escherichia coli, Pseudomonas aeruginosa, and Aspergillus Niger were kept. To create a grass culture, fresh microbial suspensions (about 10 CFU/mL) were made and evenly distributed onto sterilised agar plates using a cotton swab. A sterile cork borer was used to punch wells into the agar with a diameter of around 6 mm.

An aliquot (50-100 µL) of each sample was carefully added to the corresponding wells after various concentrations (25%, 50%, 75% and 100%) of the synthesised AgNPs were produced in appropriate solvents. DMF and methanol were used as negative controls, and chloramphenicol was utilised as a positive control. For bacterial strains, the plates were incubated at 37 ^{0}C for 24 hours, and for fungal strains, they were incubated at 28 ^{0}C for 48-72 hours. Using a Hi Antibiotic Zone Scale, the diameter of the clear zone of inhibition surrounding each well was measured after incubation to determine the antibacterial activity. The results were reported in millimetres (mm).

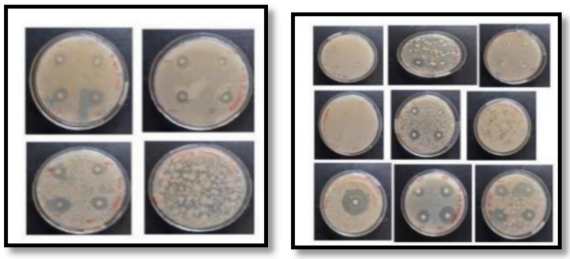

Fig.-10: Antimicrobial Action of 2-NHAgNPs & 4NHAgNPs against S. aureus, B. subtilis, E. coli, and P. Aeruginosa

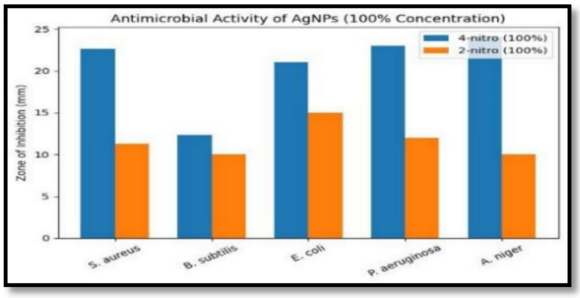

Fig.-11: Diagram of Zone of Inhibition / Gram-positive and Gram-negative Bacteria

Table-1: Results of Antimicrobial Testing

S. No.	Sample Code	*S. Aureus*	*B. Subtilis*	*E. coli*	*P. Aeruginosa*	*A. niger*
1	4-nitro (25 %)	13 mm	7.6 mm	10 mm	16 mm	16.6 mm
2	4-nitro (50 %)	13.6 mm	11 mm	12 mm	18.3 mm	18.3 mm
3	4-nitro (75 %)	15.6 mm	11.3 mm	13.3 mm	19.6 mm	23 mm
4	4-nitro (100 %)	22.6 mm	12.3 mm	21 mm	23 mm	24 mm
5	2-nitro (25 %)	-	8 mm	8 mm	7 mm	7 mm
6	2-nitro (50 %)	-	9 mm	10 mm	8 mm	10 mm
7	2-nitro (75 %)	-	10 mm	10.3 mm	8 mm	10 mm
8	2-nitro (100 %)	11.3 mm	10 mm	15 mm	12 mm	10 mm
	Chloramphenicol	NA	NA	34.3 mm	NA	NA
	DMF	-	NA	NA	NA	NA
	Methanol	-	NA	NA	NA	NA

Diameter in mm calculated by Hi antibiotic Zone Scale '-' means no zone of inhibition, NA not applicable.

Anticancer Activity

Method

The MCF- cell line in Dulbecco's Modified Eagle Medium (DMEM) supplemented with 10 % fetal bovine serum and 1% antibiotic-antimycotic was employed in this investigation. In order to get 50,000 cells per well, cells were planted. Under a 5 % CO_2 environment, cells were kept at 37 ^{0}C. Different amounts of the specified sample (100 µg/ml, 50 µg/ml, 25 µg/ml, 12.5 µg/ml, 6.25 µg/ml, 3.12 µg/ml, 1.56 µg/ml, and 0.78 µg/ml) were added to each well after 24 hours. Following 18-20 hours of incubation, the MTT assay was used to measure the sample's activity. The entire experiment was conducted in triplicate.

MTT Assay

The substrate toxicity was assessed using the MTT assay. To measure mitochondrial activity and cell viability, mitochondrial dehydrogenases convert MTT [3-(4,5-dimethylthizol-2yl)-2,5] diphenyl tetrazolium bromide; thiazolyl blue] into formazan. Each well received a 100 µL aliquot of MTT solution. The formazan crystals were dissolved by adding 100 µL to each well after the supernatant was removed following a 4-hour incubation period in a CO_2 atmosphere. A microplate reader was used to measure absorbance at 570 nm following a 10-minute shake. Corrected optical densities (OD) were used to express the results.

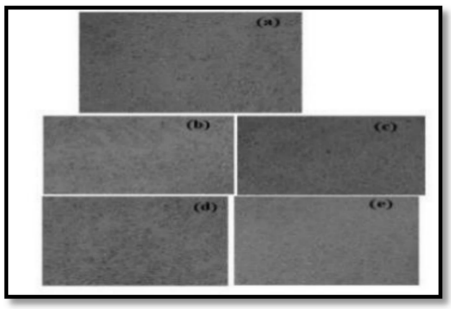

Fig.-12 (a): Before Treatment, (b, c) After Treatment of 4-NO_2 (MCF-7), (d, e) After Treatment of 2-NO_2 (MCF-7)

Table-2: Result of Anticancer Activity

$4NO_2$	
Conc.	Viability%
100	8.101473
50	9.247136
25	16.93944
12.5	57.61047
6.25	67.10311
3.125	83.96072
1.56	85.67921
0.78	127.0049

$2NO_2$	
Conc.	Viability%
100	6.792144
50	7.446809
25	9.9018
12.5	75.20458
6.25	99.09984
3.125	99.7545
1.56	100.8183
0.78	118.9034

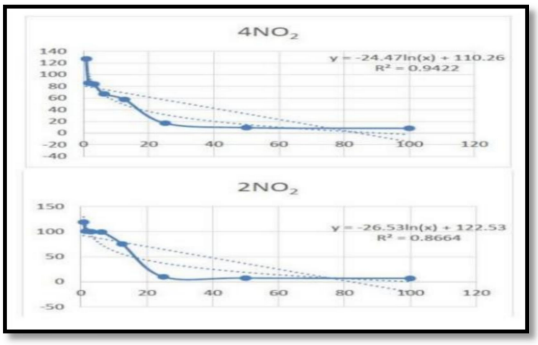

Fig.-13: Anti-cancer Activity of 2-NHAgNPs and 4-NHAgNPs

Anticancer + Antimicrobial Activity → SDG 6

CONCLUSION

This study successfully reports the synthesis of heterocyclic derivatives of aniline, 2-nitrohydrazide, and 4-nitrohydrazide, which act as both stabilising agents and reducing agents for the formation of AgNPs. The synthesised nanoparticles, designated as 2-NHAgNPs and 4-NHAgNPs, were characterised using Ultraviolet-Visible Spectroscopy, showing Surface Plasmon Resonance bands at 414 nm and 434 nm, respectively. Transmission Electron Microscopy analysis revealed particle formation within the nanoscale range, with scale bars of 2-NHAgNPs and 4-NHAgNPs for 50 nanometers and 100 nanometers. The zeta potential value was found to be +8.5 mV for 2-NHAgNPs and +2.9 mV for 4-NHAgNPs, indicating

moderate colloidal stability. The average particle size was determined to be 45.8 nanometers and 24.9 nanometers for 2-NHAgNPs and 4-NHAgNPs, respectively. The catalytic activity of 2-NHAgNPs was evaluated through the reduction of different Organic dyes, with Methyl Orange, Rhodamine B, Methyl Red, Methylene Blue, and Congo Red dyes in aqueous medium. However, catalytic degradation using 4-NHAgNPs was not feasible due to solvent incompatibility, as these nanoparticles were dispersed in DMF, in which the selected dyes are poorly soluble, whereas 2-NHAgNPs were stable in methanol and compatible with aqueous systems. MCF-7 cell line use in anti-cancer activity. Furthermore, the metal ion sensing capability of the synthesis of silver nanoparticles was investigated using Ultraviolet-Visible Spectroscopy in the presence of different metal nitrate solutions, including Co^{2+}, Pb^{2+}, Zn^{2+}, Ba^{2+}, Ca^{2+}, Mg^{2+}, K^{+}, Sr^{2+}, and Zr^{2+} ions. The sensing behaviour was observed only for 2-NHAgNPs, as effective interaction occurred in aqueous medium. 4-NHAgNPs did not exhibit sensing activity due to the solubility of metal ions in the DMF-based system. The colloid solution was evaluated opposite difference of microorganisms, including fungi, Gram-positive, and Gram-negative bacteria, with bacterial species showing fair results.

ACKNOWLEDGEMENTS

The authors gratefully acknowledge Ganpat University for providing UV–Visible and FTIR characterisation facilities, as well as metal ion detection and dye degradation analysis facilities. The authors also acknowledge SICART for providing TEM analysis facilities. Antimicrobial activity studies were carried out at Sigma University. The authors are thankful to Nirma University for providing zeta potential and particle size analysis facilities. The authors further acknowledge Gujarat Technological University, School of Applied Sciences and Technology for providing anticancer activity evaluation facilities.

CONFLICT OF INTERESTS

The author declares that there is no conflict of interest.

AUTHOR CONTRIBUTIONS

The present work is related to *SDG-6: Clean Water and Sanitation*. All the authors contributed significantly to this manuscript, participated in reviewing/editing and approved the final draft for publication. The research profile of the authors can be verified from their ORCID ids, given below:

Yesha Desai https://orcid.org/0009-0007-4404-0716
Trupti Barot https://orcid.org/0000-0003-1752-1892
Sarika Patel https://orcid.org/0000-0003-1572-0310
Nandan Pomal https://orcid.org/0000-0001-5890-3163
Dhruvansh Patni https://orcid.org/0009-0007-7321-5693
Prachi Patel https://orcid.org/0009-0001-8550-7008
Hit Kardani https://orcid.org/0009-0007-9259-9776

Cite this article as: Y. Desai *et al.*, *Rasayan J. Chem.*, 19(4), 2037-2048(2026), https://doi.org/10.31788/RJC.2026.1949946

REFERENCES

1. T. Bruna, F. Maldonado-Bravo, P. Jara, and N. Caro, *International Journal of Molecular Sciences*, **22(13)**, 7202(2021), https://doi.org/10.3390/ijms22137202
2. F. Azarbani and S. Shiravand, *Green Chemistry Letters and Reviews*, **13(1)**, 41(2020), https://doi.org/10.1080/17518253.2020.1726504
3. N. Manosalva et al., *World Journal of Microbiology and Biotechnology*, **35(6)**, 88(2019), https://doi.org/10.1007/s11274-019-2664-3
4. K. Barman, D. Chowdhury, and P. K. Baruah, *Inorganic and Nano-Metal Chemistry*, **50(2)**, 57(2020), https://doi.org/10.1080/24701556.2019.1661468

5. Y. Ren, Y. Zhang and X. Li, *Nanotechnology Reviews*, **13(1)**, 20240030(2024), https://doi.org/10.1515/ntrev-2024-0030
6. N. S. Al-Radadi and A. M. Abu-Dief, *Inorganic and Nano-Metal Chemistry*, **54(8)**, 709(2024), https://doi.org/10.1080/24701556.2022.2068585
7. E. Kabir and M. Uzzaman, *Results in Chemistry*, **4**, 100606(2022), https://doi.org/10.1016/j.rechem.2022.100606
8. S. I. Pathan, N. S. Chundawat, N. P. S. Chauhan, and G. P. Singh, *Synthetic Communications*, **50(9)**, 1251(2020), https://doi.org/10.1080/00397911.2020.1712609
9. A. Sati, T.N. Ranade, S.N. Mali, H.K.A. Yasin and A. Pratap, *ACS Omega*, **10(8)**, 7549(2025), https://doi.org/10.1021/acsomega.4c11045
10. S. Sarkar, N. T. Ponce, A. Banerjee, R. Bandopadhyay, S. Rajendran, and E. Lichtfouse, *Environmental Chemistry Letters*, **18(5)**, 1569(2020), https://doi.org/10.1007/s10311-020-01021-w
11. P.T. Tan, T.Q. Giang, T.T. Trang, V.X. Hoa, L.T. Duong, N.T. Lan, N.T. Luyen and N.V. Hao, *RSC Advances*, **16(4)**, 3296(2026), https://doi.org/10.1039/D5RA09286H
12. P.S. Pawar, S.M. Ahire, V.V. Shewale, S. Jadhav, S.K. Mahajan and D.D. Sonawane, *Research Journal of Pharmaceutical Dosage Forms Technology*, **17(4),** 279(2025), https://doi.org/10.52711/0975-4377.2025.00039
13. M. Khatami and S. Iravani, *Comments on Inorganic Chemistry*, **41(3)**, 133(2021), https://doi.org/10.1080/02603594.2021.1895127
14. A. Sharma, S. Sunny, J. Arulraj, and G. Hegde, *Nano Express*, **5(2)**, 022002(2024), https://doi.org/10.1088/2632-959X/ad4d09
15. A. Nazir et al., *Zeitschrift für Physikalische Chemie*, **235(12)**, 1589(2021), https://doi.org/10.1515/zpch-2020-1803
16. A. A. Hadi, J. Y. Ng, M. Shamsuddin, J. Matmin, and N. A. N. N. Malek, *Chemical Papers*, **76(1)**, 65(2022), https://doi.org/10.1007/s11696-021-01835-0
17. N. H. Ibrahim, G. M. Taha, N. Sh. A. Hagaggi, and M. A. Moghazy, *BMC Chemistry*, **18(1)**, 7(2024), https://doi.org/10.1186/s13065-023-01105-y
18. N. Pan et al., *Research Square*, **0**, 1(2021), https://doi.org/10.21203/rs.3.rs-216756/v1
19. I. Ashraf, A. Agarwal, N. B. Singh, and M. B. Ray, *Environmental Monitoring and Assessment*, **195(6)**, 671(2023), https://doi.org/10.1007/s10661-023-11342-2
20. M. Atasoy, D. Yildiz, İ. Kula, and A. İ. Vaizoğullar, *Food Chemistry*, **401**, 134152(2023), https://doi.org/10.1016/j.foodchem.2022.134152
21. S. Jabeen et al., *Green Processing and Synthesis*, **12(1)**, 20230167(2023), https://doi.org/10.1515/gps-2023-0167
22. D. Slimane Ben Ali et al., *RSC Advances*, **13(27)**, 18734(2023), https://doi.org/10.1039/D3RA02974C
23. H. Shahid et al., *Molecules*, **28(18)**, 6504(2023), https://doi.org/10.3390/molecules28186504
24. S. Ali et al., *Critical Reviews in Analytical Chemistry*, **53(3)**, 718–750(2023), https://doi.org/10.1080/10408347.2021.1973886
25. W. Udos et al., *Results in Optics*, **12**, 100502(2023), https://doi.org/10.1016/j.rio.2023.100502
26. F. Beck, M. Loessl, and A. J. Baeumner, *Microchimica Acta*, **190(3)**, 91(2023), https://doi.org/10.1007/s00604-023-05666-6
27. S. Tamilselvan et al., *Environmental Research*, **212**, 113585(2022), https://doi.org/10.1016/j.envres.2022.113585
28. H. Duman, F. Eker, E. Akdaşçi, A.M. Witkowska, M. Bechelany and S. Karav, *Nanomaterials*, **14(18)**, 1527(2024), https://doi.org/10.3390/nano14181527

[RJC-9946/2026]